Materials Today Chemistry 30 (2023) 101588

Contents lists available at ScienceDirect

Materials Today Chemistry

journal homepage: www.journals.elsevier.com/materials-today-chemistry/

Introducing a new perspective for the electrochemical detection of cardiac troponin I in the presence of human serum albumin (HSA), cardiac troponin C (cTnC) and C-reactive protein (CRP) based on molecular modeling and electrocatalytic activity towards ascorbic acid

Z. Mokhtari [a, b, c], S. Hashemnia [a, **], H. Khajehsharifi [b, *], S. Noroozi [a]

[a] Department of Chemistry, Faculty of Nano and Bio Science and Technology, Persian Gulf University, Bushehr 75169, Iran
[b] Department of Chemistry, Yasouj University, Under Hill, Yasouj 75918-74934, Iran
[c] Department of Chemical Industry, Technical and Vocational University (TVU), Bushehr, Iran

ARTICLE INFO

Article history:
Received 6 February 2023
Received in revised form
1 May 2023
Accepted 6 May 2023
Available online xxx

Keywords:
Cardiac troponin I (cTnI)
Molecular docking
Non-biological receptor
Layered double hydroxide nanostructures (LDHNS)
Electrochemical sensor
Ascorbic acid

ABSTRACT

Cardiac troponin I (cTnI) is a specific biomarker of myocardial damage. Several techniques have been reported for cTnI detection, which is based on immunoaffinity, aptamers, and molecular imprinting polymers. Using computational methods, we introduced a novel chemical receptor for cTnI, named tetrabromophenol blue (TBPB), which interacted with cTnI selectivity in the presence of human serum albumin (HSA), cardiac troponin C (cTnC) and C reactive protein (CRP). Employing TBPB as a chemical receptor, a novel electrochemical sensor was constructed for the electrochemical sensing of cTnI. A glassy carbon electrode surface was modified with layered double hydroxide nanostructures (LDHNS) and TBPB. The modified electrode showed electrocatalytic activity toward ascorbic acid (AA) in a phosphate buffer solution (pH 7.4). The results revealed that using AA as a signal enhancer for cTnI detection could be a good idea. The linear range (50.00−3.50 × 105 pM) and detection limit (2.77 pM) were calculated using differential pulse voltammetry to measure cTnI at the TBPB/meso-Fe/CoLDHNS/GCE in a pH 7.40 buffer solution containing 1 mM of AA. Firstly, based on our docking studies, TBPB showed a very low tendency towards HSA, cTnC, and CRP. Additionally, the selectivity of TBPB/meso-Fe/CoLDHNS/GCE for cTnI was studied electrochemically in the presence of HSA, cTnC, and CRP.

1. Introduction

With the increase in the speed of aging in societies, cardiovascular disease (CVD) has become a very important topic worldwide. Acute myocardial infarction (AMI) is a type of CVDs known as one of the principal causes of death. Therefore, early detection of AMI is essential [1,2]. The troponin complex (troponin I, T, and C) regulates cardiac muscle contraction. After a cardiac injury, the troponin complex is broken up, and the released components are distributed into systemic blood circulation [3]. Cardiac troponin I (cTnI) is known as the 'gold standard' biomarker of myocardial necrosis because it is highly sensitive to cardiac damage. Although the intravascular release of cTnI is low, it is elevated in the serum after 90 min to 3 h upon the appearance of AMI symptoms. Therefore, a simple and sensitive technique for accurately recognizing cTnI benefits the early diagnosis of AMI [4].

Up to now, many methods, including enzyme-linked immunosorbent assay (ELISA), electrochemical, fluorescent, chemiluminescent, electrochemiluminescent techniques, and surface-enhanced Raman spectroscopy (SERS), have been introduced for the recognition of cTnI. They are combined with immunosensors, aptasensors, or molecular imprinting sensors to detect cTnI. The application of these biosensors is based on biological components as recognition elements [5].

The biorecognition elements provide high selectivity and sensitivity for detecting a wide range of blood biomarkers, and making new biosensors to detect biomarkers has always been a focus of attention. In addition to the progressive development of biosensors to detect biomarkers, recent research on chemical

* Corresponding author.
** Corresponding author.
E-mail addresses: shashemnia@pgu.ac.ir (S. Hashemnia), khajeh_h@yahoo.com (H. Khajehsharifi).

https://doi.org/10.1016/j.mtchem.2023.101588
2468-5194/

molecules as non-biological receptors is also very interesting. Nandhikonda and Heagy provided a prototype to produce cTnI sensors based on non-biological recognition elements [6]. They utilized the bioinformatic principles and developed a fluorescent probe for cTnI detection. According to the significant characteristics of the electrochemical sensors, including high sensitivity, we have proposed an electrochemical sensor for cTnI detection using a redox chemical receptor. Utilizing molecular docking investigations, Tetrabromophenol blue (TBPB) was chosen as a chemical receptor. This study used computational molecular docking to select an appropriate chemical compound as a non-biological recognition element in the proposed electrochemical sensor.

TBPB dye is a member of benzofurans. Its chemical structure consists of three parts, 1, 2, 3, 4 -tetrabromobenzene, sulfonic acid, and 2-6-dibromophenol [7]. The biochemical investigations of TBPB show that electrostatic and hydrophobic interactions are involved in the TBPB binding to proteins. Although TBPB is used as a pH indicator dye (e.g. testing proteinuria and renal pathology), few reports show it being used as a redox indicator [8].

Utilizing nanoparticles is a favorite strategy in electrochemical sensors to enhance their sensitivity. Recently, layered double hydroxide nanostructures (LDHNS) have been attaining much attention due to their large surface area, good electrochemical properties, and adsorption capacity. They consist of positively charged brucite-like layers. These layers are a mix of metal hydroxides, which are separated by intercalated hydrated anions. The general formula of $[M^{2+}{}_{(1-x)}\, M^{3+}{}_{(x)}\, (OH)_2]^{x+}\, [(A^{n-})_{x/n}.\, mH_2O]$ has been defined for LDH structures, where M^{2+} and M^{3+} are bivalent and trivalent metal cations, respectively, and A^{n-} depicts the interlayer anion [9,10]. Considering the porous morphology of LDHNS and their high adsorption capacity for dyes, we designed an electrochemical sensor for cTnI detection using a glassy carbon electrode modified with meso-Fe/Co layered double hydroxide nanostructures and TBPB (TBPB/meso-Fe/Co LDH NS/GCE). In this way, we enhanced the electrochemical performance of a TBPB dye on an electrode surface by using LDHNS as an adsorbent of the dye. However, there was still a need to amplify the electrochemical signal to achieve the desired sensitivity. In these conditions, the results exhibited that the proposed modified GCE showed an electrocatalytic activity toward anodic oxidation of ascorbic acid (AA). We found that the electrocatalytic activity of the modified electrode toward AA oxidation was changed in the presence and absence of cTnI, and the changes in the anodic peak current of AA at different concentrations of cTnI have been measured. These changes provide a suitable sensitivity to construct a sensor for cTnI.

Ascorbic acid is a redox-active biological compound and can undergo an irreversible oxidation change to dehydroascorbic acid. The irreversible electrocatalytic oxidation of AA shows an irreversible cyclic voltammogram with an oxidation peak [11]. Although there are some studies on the electrochemical detection of AA in aqueous solutions using modified electrodes with different dyes [12–14], to the best of our knowledge, none of the studies has used TBPB/meso-Fe/Co LDH NS/GCE as a modified electrode for sensing AA.

Therefore, in this research, for the first time, TBPB was introduced as a non-biological redox-active receptor for cTnI using molecular docking simulations and electrochemical study. Furthermore, by considering possible interactions between TBPB and cTnI, as well as the catalytic effect of TBPT on the anodic oxidation peak current of AA, we tried to determine cTnI in the absence and presence of human serum albumin (HSA), C-reactive protein (CRP) and cardiac Troponin C (cTnC) through research the change in the anodic oxidation peak currents of AA on the modified electrode surface.

2. Molecular modeling and experimental methods

2.1. Material and apparatus

The information about the chemicals and apparatus is represented in the supplementary material (section S1).

2.2. Molecular modeling

More information is represented in the supplementary material (section S2).

2.3. Synthesis of meso-Fe/Co layered double hydroxide nanostructures (meso-Fe/Co LDH NS)

The information about the synthesis is represented in the supplementary material.

2.4. Preparation of the non-biological electrochemical sensor for cTnI

2.4.1. Modification of the GCE surface with meso-Fe/Co LDH NS

A suspension containing 1.5 mg/mL of meso-Fe/Co LDH NS in water was sonicated for 90 min. Then, 10 μL of the homogeneous suspension was poured on the GCE surface and dried in a vacuum for 1 h. The resulting electrode was called meso-Fe/Co LDH NS/GCE.

2.4.2. Modification of the electrode surface with TBPB

The meso-Fe/Co LDH NS/GCE was immersed in a TBPB solution (150 μM, PBS pH 4.3) for 2 h to obtain TBPB/meso-Fe/Co LDH NS/GCE. In order to optimize the pH and concentration of the TBPB solution and reach the optimum immersion time, the electrochemical response of the modified electrodes was explored under different conditions. As a control condition, the bare GCE was immersed in TBPB 150 μM, PBS pH 4.30) for 2 h to get TBPB/GCE.

2.4.3. Electrochemical behavior of ascorbic acid (AA) on the TBPB/meso-Fe/Co LDH NS/GCE

The electrochemical behavior of AA on the modified GCE was investigated using cyclic voltammetric and differential pulse voltammetric techniques. The AA solution was titrated in the PBS (100 mM, pH 7.40), and the corresponding voltammograms were recorded. Bare GCE, TBPB/GCE, and meso-Fe/Co LDHNS/GCE were also used to investigate the AA redox reaction under the control probe conditions.

2.4.4. Detection of cTnI on the TBPB/meso-Fe/Co LDH NS/GCE in the AA electrolyte solution

In the next step of the procedure, AA was applied as a signal amplifier to construct a non-biological electrochemical sensor for cTnI detection. For this purpose, the modified electrodes (TBPB/meso-Fe/CoLDH NS/GC) were incubated with different concentrations of cTnI (0.0, 50.0, 80.0×10^1, 20.0×10^3, 60.0×10^3, $1.4 \times 10^5$and 3.5×10^5 pM) for 2 h (to obtain significant interactions between TBPB and cTnI). Then, the electrocatalytic activity of the electrode toward AA oxidation was investigated in the presence and absence of cTnI by DPV in the electrolyte solution containing AA 1.00 mM, and the change in the anodic peak current of AA at different concentrations of cTnI was measured. To further validate the role of AA in the electrode response to cTnI, a control experiment was done by incubating the modified electrodes in the cTnI solutions and recording the corresponding voltammograms in an electrolyte solution without AA.

3. Results and discussion

Though aptamers and antibodies are favored receptors to establish electrochemical biosensors, a paradigm shift focusing on replacing biological molecules with chemical receptors would be valuable. Combining the molecular docking, this paper proposes a redox-active receptor to detect cTnI. Molecular docking was carried out to evaluate the affinity of ligands and cTnI. The stronger the ligand-cTnI binding, the higher the affinity and the more stable the complex obtained. The lowest docking energies of the tested ligands have redox activity, and the results are shown in Table S2 (Supplementary Information). The best cTnI-ligand complex was achieved by comparing several scoring criteria, such as Gibbs free energy, binding site, and hydrogen binding. The most satisfactory docking results corresponded to the cTnI complexes with three redox compounds 7 (tetrabromophenol Blue (TBPB)), 8 (Bromocresol Green), and 9 (Bromocresol Purple) showed affinity values of −6.97, −5.66 and −6.17 kcal/mol, respectively. These ligands entered cTnI through H-binding and van der Waals' force, where amino acid residues such as Asp105, Glu109, Lys106, and Arg103 play important roles in the binding cavity (Fig. 1B). Here, it is important to remark that the best ligand as a receptor is that not only shows the strongest affinity to cTnI, but also displays a low tendency for complexation with other proteins such as HSA, cTnC, and CRP, which exist in human serum. Therefore, the affinity of the three ligands mentioned above to HSA, CRP, and cTnC proteins will also be investigated.

3.1. Molecular docking analysis of ligands with CRP, TnC, and HSA (computational approach for selectivity considerations of the sensor)

Although a high level of CRP could be represented through cardiac damage, this is not specific to cardiac complications because an elevated CRP level is also associated with chronic renal insufficiency and a serious bacterial infection of the lung and the urinary tract [16]. Cardiac injuries cause the release of troponins in circulation in different forms, including the complex of cTnI/cTnT/cTnC and free molecules. cTnI and cTnT have been considered to be specific biomarkers of myocardial injury. Troponin C is not specific to cardiac muscles because it is also found in the skeletal muscle [17]. Following myocardial damage, CRP and TnC proteins could interfere with cTnI analysis. HSA was also examined for selectivity. To verify the low affinity of chosen ligands with the above-mentioned proteins (CRP, TnC, and HSA) and select one of them as the chemical diagnosing element of the sensor, molecular docking analysis was employed. The results are shown in Tables S3–S11. The molecular docking of ligands to CRP (3L2Y) shows the lowest affinity for ligands 6 (Bromophenol blue), 7, and 8, and the lowest affinity to cTnC was shown for ligand 7. The results are related to the docking analysis of the ligands with three cTnC PDB codes to attain the different binding sites. Then, to predict the affinity of the ligands to HSA, they were docked into HSA using four different types of PDB codes (3LU6, 3LU7, 3LU8, 5GIY). So, the probable different binding sites were analyzed. These results revealed that ligand 7 had the lowest affinity to HSA than the other ligands. For more information concerning docking results of ligands with CRP, cTnC, and HSA, see Supplementary Materials (Sections S2–S5). Based on the docking results, whereas ligand 7 showed a high affinity for cTnI, it displayed a low tendency towards CRP, cTnC, and HSA. Fig. 1 presents the docked structure and binding site of ligand 7 (TBPB) to cTnI. The cTnI detection concerning the electrochemical behavior of TBPB was shown in Scheme 1, where TBPB was used as the cTnI receptor.

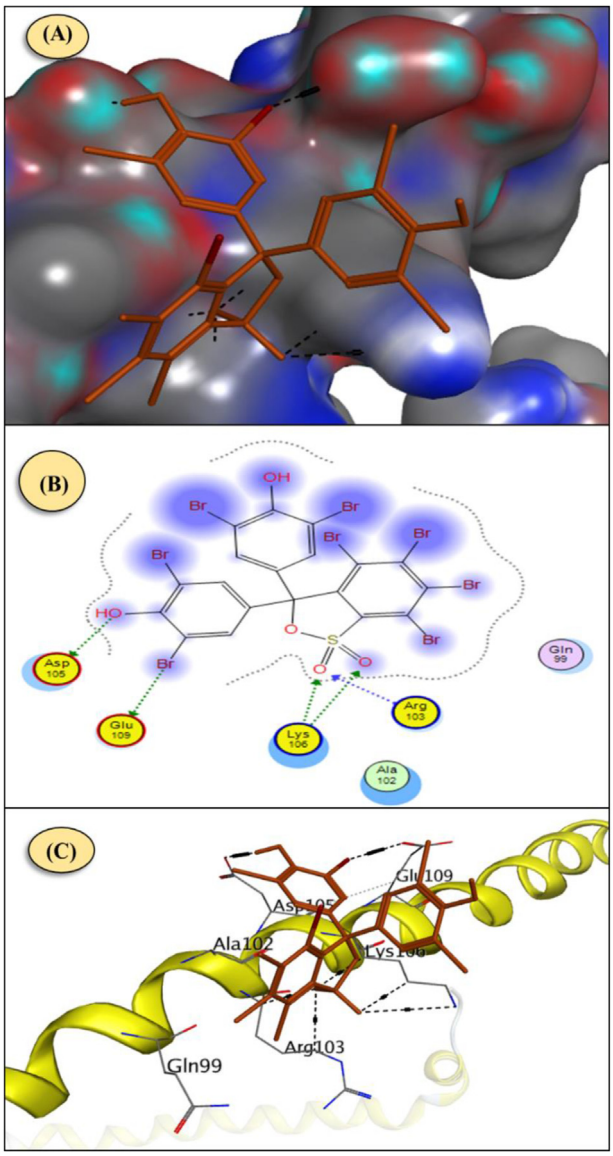

Fig. 1. Docking state with the lowest binding free energy of TBPB into cTnI, (A) a receptor surface of cTnI and TBPB represented as sticks in the binding cavity and showing hydrogen bond interaction (black dashed lines), (B) 2-dimensional TBPB interaction and residues surrounding the binding pocket, (C) 3-dimensional model of hydrogen bond interaction of TBPB with cTnI.

3.2. Nanostructure characterization

The XRD pattern of meso-Fe/Co LDH NS (Fig. 2A) represents a series of (003), (006), and (110) peaks at 2Θ about 11.45°, 23.00° and 59.87°, respectively, which is by diffraction characteristics of the hydrotalcite-like structure of LDHs [15]. The morphologies and structures of the meso-Fe/Co LDHNS and meso-Fe/Co LDHNS coated with TBPB (TBPB/meso-Fe/Co LDH NS) were analyzed by TEM and FESEM. The TEM image (Fig. 2B) reveals that meso-Fe/Co LDHNS was composed of wrinkles, which may be aggregates of layers of various sizes growing in different directions, thus forming 3D spherical nanostructures with an average size of 45 nm (Fig. 2C). These spherical nanostructures exist in various aggregates, which contain mesoporous materials. The image in Fig. 2E shows the surface of TBPB/meso-Fe/Co LDHNS in a different shape from that in Fig. 2D. It is composed of many wrinkles and forms a 3D porous structure all over the whole surface, which could be a result of the

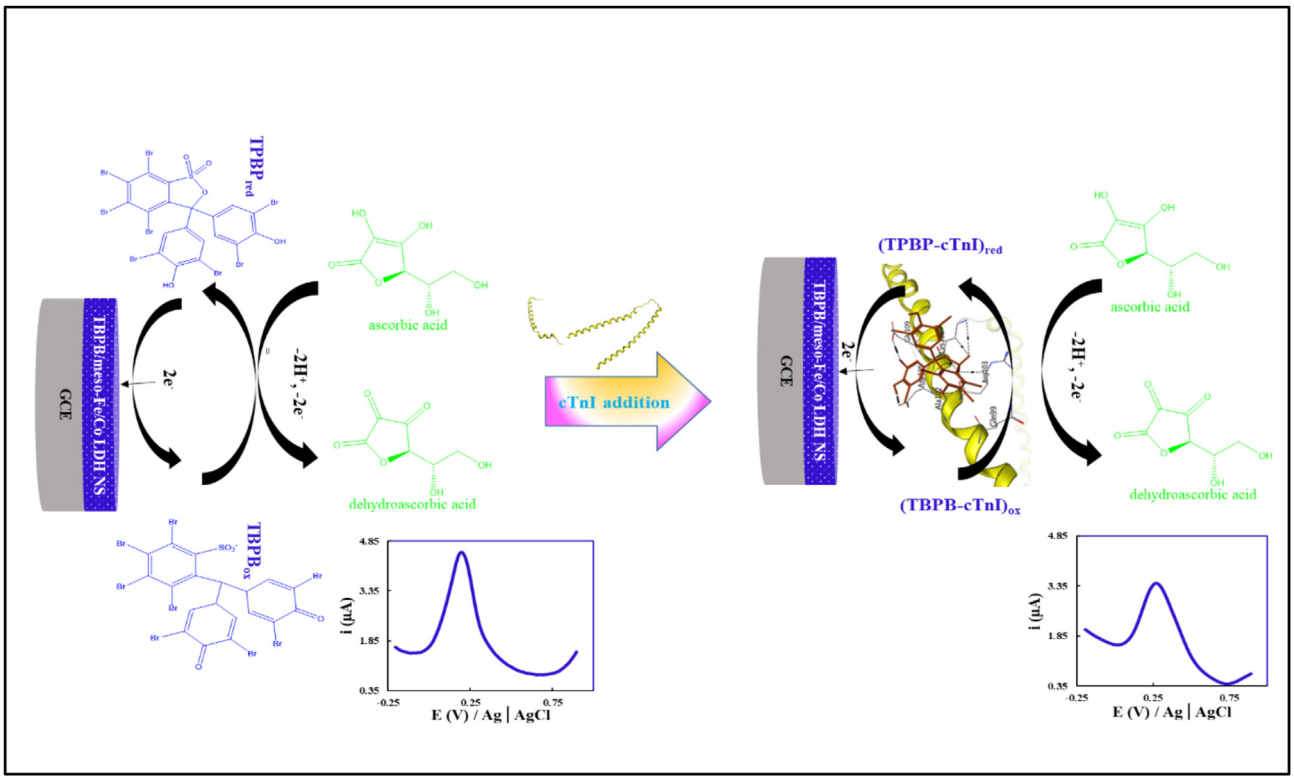

Scheme 1. Representation of the electrocatalytic oxidation of AA on the TBPB/meso-Fe/Co LDHNS/GCE (left) and the decrease in the AA electrocatalytic oxidation peak after the cTnI addition that influenced the redox behavior of TBPB by inducting probable interactions.

surface coating with TBPB. Furthermore, this special modification is useful for the development of electrochemical performance [18,19]. Fig. 2F presents the N_2 adsorption−desorption isotherms of meso-Fe/Co LDHNS and TBPB/meso-Fe/Co LDHNS. To IUPAC classification, both samples show the conventional type IV isotherms with apparent hysteresis loops (type H-3) at a relative pressure of p/p° 0.4−1.0 m, indicating the mesoporous structure of the samples. However, as the TEM and SEM images show, deep hysteresis loops correspond to the slit-shaped pores of the aggregates of plate-like wrinkles. In addition, the sharp peaks of the BJH curves for pore diameter distributions (Fig. 2G) can be seen as centering at 6.30 nm and 7.26 nm for meso-Fe/Co LDH NS, and TBPB/meso-Fe/Co LDHNS, respectively. Based on the BET analysis, the specific surface area and pore volume reduced from 139.60 m^2/g and 0.17 cm^3/g to 63.67 m^2/g and 0.09 cm^3/g, respectively, after meso-Fe/Co LDHNS was exposed to the dye, implying that a smoother pore surface was obtained as the dye molecules filled the pores [15,20].

3.3. Characterization of the modified GCEs

Each step in the modification process was assessed by CV and EIS. According to the cyclic voltammograms of Fig. 3A, the peaks of TBPB (Ec = 0.25 V, Ea = 0.29 V) significantly increased for TBPB/meso-Fe/Co LDHNS/GCE (Curve d) vs. TBPB/GCE (Curve c), while the meso-Fe/Co LDHNS was electrochemically inactive (curve b). The peak growth could be considered a consequence of the effective concentration of TBPB at the GCE surface, which resulted from the desirable performance of meso-Fe/Co LDHNS to increase the electrode surface area. The surface modification was confirmed by EIS data. By equivalent circuit fitting, the Nyquist plots were analyzed (Table S12), and the charge transfer resistance (R_{ct}) was obtained. Based on the Nyquist plots (Fig. 3B), due to the low conductivity, the meso-Fe/Co LDH NS modification remarkably increased the semicircle diameter of meso-Fe/Co LDH NS/GCE (R_{ct} = 2.210 kΩ), compared to the bare GCE (R_{ct} = 0.163 kΩ). It should be noted that, for TBPB/meso-Fe/Co LDH NS/GCE, the TBPB molecules increase the surface conductivity, causing a decrease in the R_{ct} to 0.672 kΩ and semicircle diameter compared to meso-Fe/Co LDH NS/GCE [21].

3.4. Evaluation of the effects of operating variables

The meso-Fe/Co LDHNS concentration on the modified GCE surface was an important variable for the design of the proposed electrochemical sensor. For this purpose, the decrease in the R_{ct} for TBPB/meso- Fe/Co LDH NS/GCE, in comparison with meso-Fe/Co LDH NS/GCE, was investigated (Fig. 3C).

The Nyquist plots showed that the semicircle for meso-Fe/Co LDH NS/GCE kept increasing as the concentration of meso-Fe/Co LDH NS grew from 0.5 to 4.0 mg/mL. This was due to an increasing Rct value. However, after the adsorption of the TBPB, the semicircle diameter decreased for all of them. The lowest R_{ct} (0.67 kΩ) for TBPB/meso-Fe/Co LDH NS/GCE was obtained at a concentration of 1.5 mg/mL of meso-Fe/Co LDH NS (Fig. 3D). This indicated that 1.5 mg/mL of meso-Fe/Co LDH NS/GCE had a high enough tendency for TBPB adsorption. The pH of the TBPB solution to adsorb on the meso-Fe/Co LDH NS/GCE surface is another important parameter, as it strongly affects the anodic peak current of TBPB. Fig. S10 indicates that the TBPB anodic peak intensity was low at the high pH values and high at the low ones. The maximum peak current was observed at the pH of 4.30 for the TBPB solution, indicating the maximum adsorption of TBPB on the meso-Fe/Co LDH NS/GCE at this pH value [22,23]. The concentration of the TBPB solution was also investigated. As shown in Fig. S11A and B, with an increase in the TBPB concentration from 10 to 300 μM, the CV peak currents kept increasing until 150 μM, while after that,

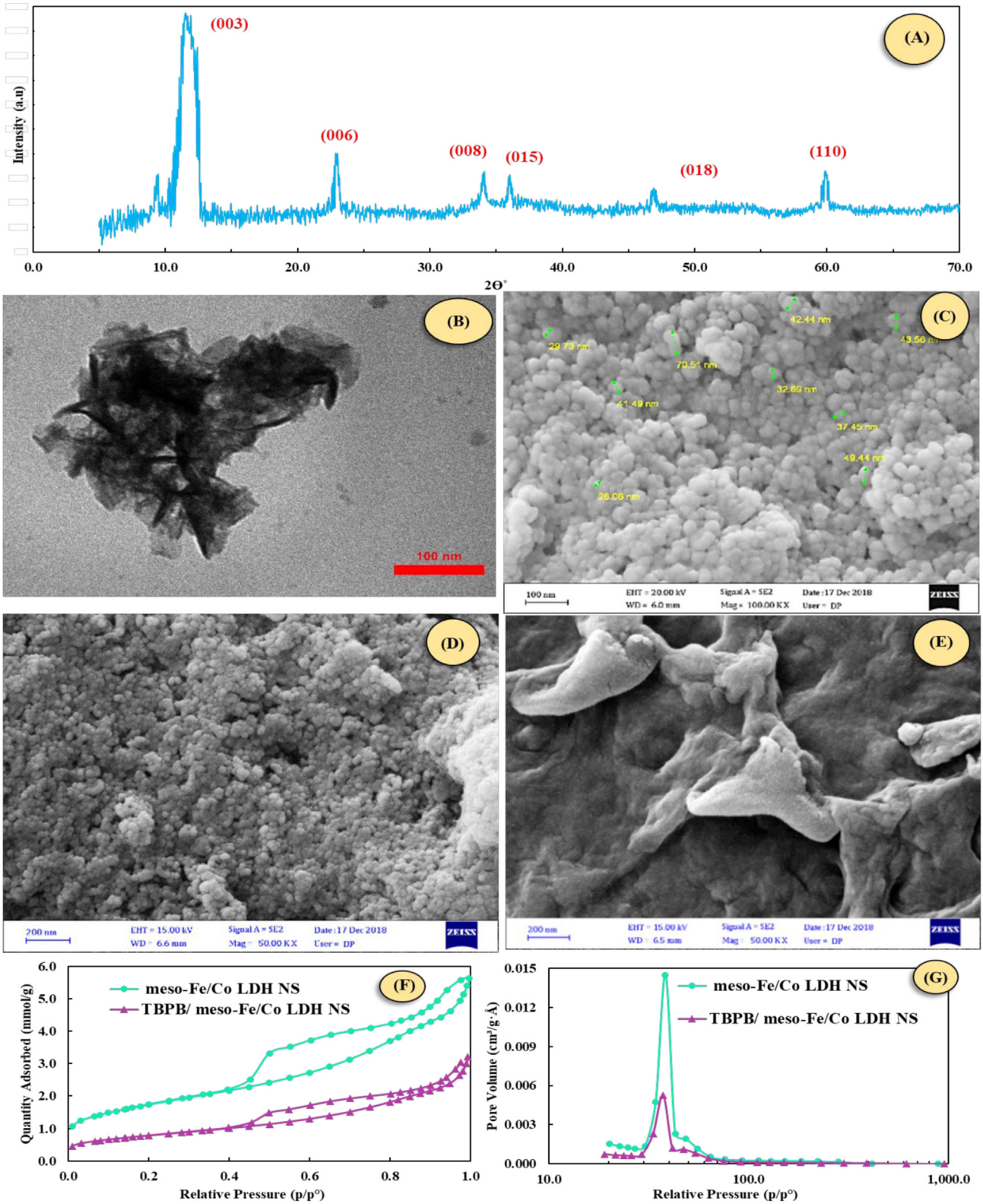

Fig. 2. (A) XRD pattern, (B) TEM image, (C) and (D) FESEM images with two magnifications of meso-Fe/Co LDHNS, (E) FESEM image of TBPB/meso-Fe/Co LDHNS, (F) N2- adsorption-desorption isotherms and (G) BJH curves of meso-Fe/Co LDHNS and TBPB/meso-Fe/Co LDHNS.

they remained unchanged, suggesting that 150 μM of TBPB was enough to coat the modified GCE. The time for the adsorption of TBPB on the meso-Fe/Co LDH NS/GCE is another variable that was optimized, and 2 h were chosen (Fig. S11C and D). (More information is presented in Supplementary Data).

The electrochemical activity of the modified electrodes was investigated by introducing ascorbic acid (AA) to the electrolyte solution. In the presence of AA, a weak anodic peak was observed in the cyclic voltammogram for GCE. For meso-Fe/Co LDH NS/GCE and TBPB/meso-Fe/Co LDH NS/GCE, the anodic peaks increased, but the

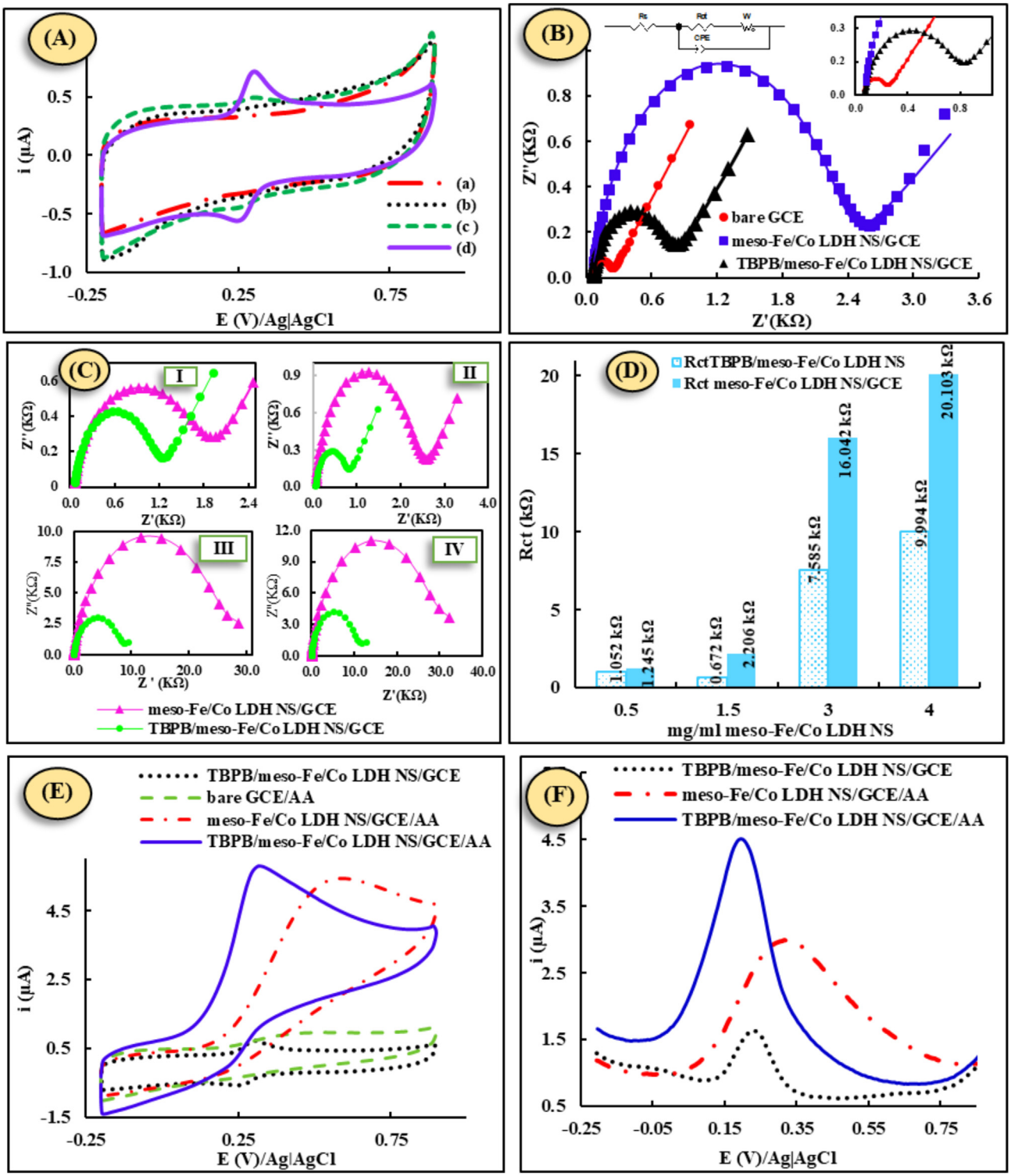

Fig. 3. (A) Cyclic voltammograms of (a) bare GCE, (b) meso-Fe/Co LDHNS/GCE, (c) TBPB/GCE, (d) TBPB/meso-Fe/Co LDHNS/GCE in an electrolyte solution containing PBS (100 mM, pH 7.40) and KCl (100 mM), with a scan rate of 100 mV/s, (B) Nyquist plots of bare GCE, meso-Fe/Co LDHNS/GCE and TBPB/meso-Fe/Co LDHNS/GCE (inset of the curve: the equivalent circuit used to fit data), (C) Nyquist plots of meso-Fe/Co LDH NS/GCE and TBPB/meso-Fe/Co LDHNS/GCE using different concentrations of meso-Fe/Co LDH NS ((I) 0.5, (II) 1.5, (III)3.0, (IV)4 mg/mL) to modify the GCE surface in electrolyte solution containing ferro/ferricyanide ($[Fe(CN)_6]^{3-/4-}$) couple (50 mM) and KCl (100 mM), frequency range between 50 mHz and 10 kHz, (D) Column curve of comparing the Rct obtained from the Nyquist plots of Fig.C, (E) cyclic voltammograms of TBPB/meso-Fe/Co LDHNS/GCE in electrolyte solution in the absence of AA, and bare GCE, meso-Fe/Co LDHNS/GCE, TBPB/meso-Fe/Co LDHNS/GCE in the electrolyte solution (PBS 100 mM, pH 7.4) and KCl (100 mM)) containing AA 1 mM (at a scan rate of 100 mV/s), (F) DPV anodic peaks of the TBPB/meso-Fe/Co LDHNS/GCE in the absence of AA and meso-Fe/Co LDHNS/GCE, TBPB/meso-Fe/Co LDHNS/GCE in the presence of AA 1 mM.

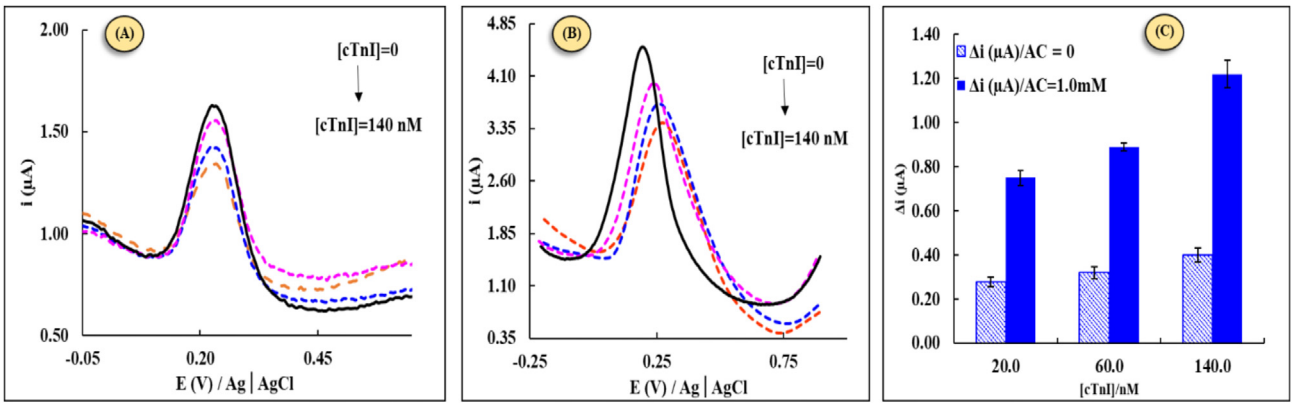

Fig. 4. (A) Anodic differential pulse voltammograms of the TBPB/meso-Fe/Co LDH NS/GCE incubated at different concentrations of cTnI (0.0, 20.0, 60.0, and 140.0 nM) [The peaks were recorded in an electrolyte solution containing PBS (100 mM, pH 7.40) and KCl (100 mM) (in the absence of AA), and (B) in the presence of AA (0 mM), (C) the column curve to compare the changes in the anodic peak currents of Figs. (A: in the absence and B: in the presence of AA).

intensity of the former at $Ep_a = 0.55$ V was lower than the latter at $Ep_a = 0.31$ V. By comparison, the current intensity was increased, and the overvoltage was reduced, implying higher electrocatalytic activity of the film containing TBPB. (TBPB/meso-Fe/Co LDH NS/GCE) (Fig. 3E and F) [24,25]. The suggested electrocatalytic mechanism is shown in Scheme 1.

CVs of TBPB/meso-Fe/Co LDH NS/GCE in the presence of 1 mM AA (TBPB/meso-Fe/Co LDH NS/GCE/AA) were obtained at different scan rates (Fig. S13). As shown in Fig. S13B, the curve of the logarithm of the anodic peak currents vs. the logarithm of the scan rate (Log i_{pa} − Log v curve) offers a line with a slope of 0.3249, which reveals that the electrocatalytic process was a diffusion-controlled reaction. In addition, a slope of 0.8464 for the Log i_{pc} −Log v curve indicates that the electrochemical reaction of TBPB was a surface-controlled reaction [26]. Considering the electrocatalytic activity of the TBPB/meso-Fe/Co LDHNS/GCE in the PBS containing 1 mM AA, the anodic peak current was enhanced compared with the absence of AA. Thus, the TBPB/meso-Fe/Co LDHNS/GCE in the electrolyte solution containing AA 1.00 mM was utilized to detect cTnI in the following assays electrochemically. In this case, during the voltammetric measurement, the TBPB redox molecules were involved in interaction with cTnI, and the electrochemical behavior of TBPB and AA electro-oxidation were affected by this interaction.

3.5. Investigation of the effect of AA on the improvement of the TBPB/meso-Fe/Co LDH NS/GCE response to determining the cTnI

After incubation of the modified electrode, TBPB/meso-Fe/CoLDHNS/GCE in the cTnI solutions at concentrations of 0.0, 20.0, 60.0, and 140.0 nM, the anodic differential pulse voltammograms of the electrode in the absence (Fig. 4A) and presence (Fig. 4B) of AA in the electrolyte solution were recorded. As seen in Fig. 4A, in the absence of AA, the observed oxidation peaks are related to the TBPB, which were affected by the different concentrations of cTnI and reduced by increasing the cTnI concentrations. Based on the molecular docking results, the decrease of the TBPB oxidation peak in the presence of cTnI can be attributed to the possibility of the hydrogen bonding between the cTnI side chains as well as the hydroxyl and sulfate groups of TBPB, while in Fig. 4B, the voltammograms were recorded in the presence of AA (1.0 mM). In these voltammograms, as discussed above, the observed peak was related to the electrocatalytic oxidation of AA at the TBPB/meso-Fe/Co LDH NS/GCE.

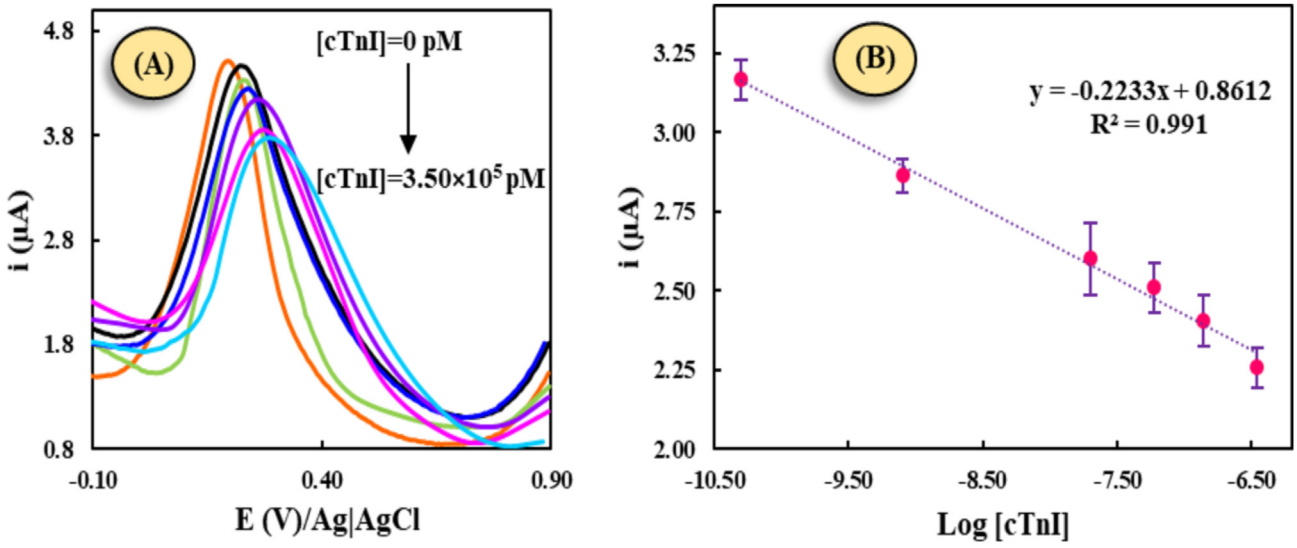

Fig. 5. (A) DPV anodic peaks of the TBPB/meso-Fe/Co LDH NS/GCEs before and after incubation in different concentrations of the cTnI (50.0, 80.0 × 10^1, 20.0 × 10^3, 60.0 × 10^3, 1.4 × $10^5$and 3.5 × 10^5 pM) recorded in the electrolyte solution (PBS pH 7.40 and KCl 100 mM) containing AA 1.0 mM, (B) calibration curve for cTnI detection (the currents were obtained from Curve (A)).

Table 1
Comparison of the performance of some designed sensors for cTnI.

Sensor type	Recognition element	Signal amplification method	Detection limit (ng/ml)	Reference
Fluorescence	Abiotic Probe (N-aryl- 2,3-naphthalimide)	–	–	[6]
Electrochemical	Antibody	(enzyme catalytic performance) H_2O_2- horseradish peroxidase (HRP) - hydroquinone (HQ.)	1.70×10^{-3}	[27]
Electrochemiluminescence	synthesized short linear specific binding peptide (FYSHSFHENWPSK)	Signal Reagent-Encapsulated Liposomes	4.50×10^{-3}	[28]
Colorimetric	Strong complex forming tendency between heparin and cTnI	Gold nanorods (AuNRs)	4.00×10^{-1}	[29]
Electrochemical	13-amino acid peptide (FYSHSFHENWPSC)	triangular icicle like gold nanostructure	9.00×10^{-4}	[30]
Electrochemical	Aptamer	Silica nanoparticles	2.40×10^{-2}	[31]
Electrochemical	MIP	Multiwalled carbon nanotubes (MWCNTs), chitosan (CS), glutaraldehyde (GA) composites	8.00×10^{-4}	[32]
Electrochemical	Abiotic Probe (tetrabromophenol Blue (TBPB)	Electrocatalytic activity of the modified electrode toward Ascorbic Acid oxidation	6.65×10^{-2}	This work

The changes in the peak current intensities were greater than the current intensities obtained in the absence of AA. Accordingly, the results show that the effect of possible interactions of cTnI - TBPB on the electrochemical behavior of TBPB in the presence of AA was more significant, and, therefore, the presence of AA would increase the sensitivity of the designed probe for cTnI detection.

3.6. Use TBPB/meso-Fe/Co LDH NS/GCE/AA as an electrochemical probe to detect cTnI

The anodic differential pulse voltammograms of TBPB/meso-Fe/Co LDH NS/GCE/AA for different concentrations of cTnI were obtained under the optimum conditions. For this purpose, TBPB/meso-Fe/Co LDH NS/GCE was incubated at various concentrations of cTnI ($50.00-3.50 \times 10^5$ pM), and the corresponding voltammograms were recorded in an electrolyte containing PBS pH 7.40 and AA 1.00 mM. The enhanced characteristic peak current of AA at the TBPB/meso-Fe/Co LDH NS/GCE surface was decreased as the cTnI concentration increased to 3.50×10^5 pM (Fig. 5A). When cTnI was increased and the current decreased, the anodic potential shifted to positive potentials, confirming the probable interactions between cTnI and TBPB. Fig. 5B represents the corresponding logarithmic calibration curve (I_{pa} (μA) = $-0.2233 \times$ Log [cTnI]) + 0.8612, $R^2 = 0.991$). The detection limit was estimated to be 2.77 pM based on the formula $3s_b/m$, where s_b is the standard deviation in 3 replicate measurements of the blank, and m is the slope of the calibration curve (0.2233 μA/pM).

In the first effort to choose a suitable ligand with a high tendency to cTnI, TBPB was selected as the affinity ligand because of its low tendency to some other proteins based on the docking study. Moreover, HSA, CRP, and cTnC were chosen to check the selectivity in experimental conditions. For this purpose, the prepared modified electrodes were incubated in the solutions containing 20.0×10^3 pM of cTnI in the presence of 20.0×10^3 pM. Then, the oxidation differential pulse voltammograms of the modified electrodes were recorded in the electrolyte solution containing AA (1.00 mM). The changes in the oxidation peak currents were relatively close to those of cTnI alone (Fig. S14). Therefore, these results display the selectivity of the proposed probe to determine cTnI in the presence of the HSA, CRP, and cTnC proteins (Fig. S14, the column curve).

The reproducibility assessment of the designed cTnI sensor was investigated using three modified electrodes. Under the same conditions, the three TBPB/meso-Fe/Co LDH NS/GCEs were prepared and incubated in the cTnI solution (20.0×10^3 pM). Then, the oxidation peaks were recorded (in the presence of AA 1.00 mM) before and after the incubation process (Fig. S15). The relative standard deviation (RSD %) was about 5.21%, which shows acceptable reproducibility (Table S13).

The peak-to-peak stability/TBPB/meso-Fe/Co LDH NS/GCE was evaluated by recording the cyclic voltammograms in the PBS pH 7.40 and KCl 100 mM). As seen in Fig. S16(A), there were no remarkable changes in the peaks before and after 10 cycles. The stability of the TBPB/meso-Fe/Co LDH NS/GCE was analyzed for 5, 10, 20, and 30 days, which was stored in the PBS solution at pH 4.30 and 5 °C. After each period, the anodic peak currents were obtained in the electrolyte solution containing PBS pH 7.40 and KCl (Fig. S16(B)). The percentage changes of the peak current are given in Table S14. The results show relative stability (73.23%) in the peak currents after 30 days. Utilizing the standard addition method, the recoveries were 96.67%–103.57% when the diluted serum samples spiked with 1.23×10^{-3} - 3.50 μg/mL cTnI (Table S15).

4. Conclusion

The reports for cTnI sensors are vast. Researchers have introduced very different types of sensors based on aptamers, antibodies, molecularly imprinting polymers (MIPs), peptides, and other non-biological molecules [6,27–32]. Using different sensors, the detection limits have been explored in different ranges. Each of the introduced sensors has its advantages, but usage may be limited by either their sensitivity or cost. As shown in Table 1, besides the acceptable detection limit, the proposed sensor in this work has the advantages of simplicity, cheapness, and stability.

In designing this non-biological electrochemical probe, at first, docking studies were employed to determine the best receptor for cTnI in the presence of some other proteins, such as HSA, CRP, and cTnC. According to our molecular docking evaluations, TBPB (as a redox-active molecule) can be docked into the cTnI structure with more affinity to the amino acid sequences of 99–109. These interactions consist of the Asp 105, Glu 109, Lys 106, Arg 103, Ala 102, and Gln 99 residues with the hydroxyl, sulfate, and bromide groups of TBPB. The binding energy value was obtained to be −6.97 kCal/mol. However, based on the docking studies, TBPB did not show a high tendency for docking into HSA, CRP, and cTnC. Therefore, the electrochemical investigations employed it as a non-biological receptor to determine cTnI in the presence of the above-mentioned proteins. In the following step, the working electrode (GCE) was modified with nanoparticles to improve the electrochemical sensor's performance. Considering the porous morphology of the synthesized meso-Fe/Co LDH NS and their high adsorption capacity for dyes, GCE was modified by meso-Fe/Co LDH NS to maximize the absorption of TBPB.

Moreover, our studies reveal that TBPB/meso-Fe/CoLDHNS/GCE show an electrocatalytic activity towards ascorbic acid (AA) in phosphate buffer solution (pH 7.4). Considering the decrease in the DPV peak currents in the presence of cTnI, compared to the absence of cTnI, AA could be a good choice to enhance the electrochemical

signal. The detection was based on the electrochemical oxidation of AA by TBPB. In a way, the cTnI binding by TBPB affected the electrochemical oxidation of AA. The sensor displayed a good linearity (50.00–3.50 × 10^5 pM) and detection limit (2.77 pM) for cTnI. Interference from HSA, CRP, and cTnC proteins was minimal. Although much remains to be studied, utilizing such systems could provide possibilities for introducing chemical receptors as blood markers.

Credit author statement

Habibollah Khajehsharifi: Supervision, **Sedigheh Hashemnia:** Supervision, **Zaynab Mokhtari:** Project administration, **Soodeh Noroozi:** Visualizing.

Declaration of competing interest

The authors declare that they have no known competing financial interests or personal relationships that could have appeared to influence the work reported in this paper.

Data availability

The authors are unable or have chosen not to specify which data has been used.

Acknowledgments

This research was supported by Yasouj University and the Persian Gulf University of Bushehr, Iran.

Appendix A. Supplementary data

Supplementary data to this article can be found online at https://doi.org/10.1016/j.mtchem.2023.101588.

References

[1] X. Jiang, H. Wang, Y. Chai, W. Shi, R. Yuan, High-efficiency CNNS@ NH2-MIL (Fe) electrochemiluminescence emitters coupled with Ti3C2 nanosheets as a matrix for a highly sensitive cardiac troponin I assay, Anal. Chem. 92 (2020) 8992–9000, https://doi.org/10.1021/acs.analchem.0c01075.
[2] H. Dong, L. Cao, Z. Tan, Q. Liu, J. Zhou, P. Zhao, P. Wang, Y. Li, W. Ma, Y. Dong, A signal amplification strategy of CuPtRh CNB-embedded ammoniated Ti3C2 MXene for detecting cardiac troponin I by a sandwich-type electrochemical immunosensor, ACS Appl. Bio. Mater. 3 (2019) 377–384, https://doi.org/10.1021/acsabm.9b00863.
[3] L. Babuin, A.S. Jaffe, Troponin: the biomarker of choice for the detection of cardiac injury, Can. Med. Assoc. J. 173 (2005) 1191–1202, https://doi.org/10.1503/cmaj/051291.
[4] C. Bao, X. Liu, X. Shao, X. Ren, Y. Zhang, X. Sun, D. Fan, Q. Wei, H. Ju, Cardiac troponin I photoelectrochemical sensor: {Mo368} as electrode donor for Bi2S3 and Au co sensitized FeOOH composite, Biosens. Bioelectron. 157 (2020), 112157, https://doi.org/10.1016/j.bios.2020.112157.
[5] Z. Yuan, L. Wang, J. Chen, W. Su, A. Li, G. Su, P. Liu, X. Zhou, Electrochemical strategies for detection of cTnI, Analyst 146 (2021) 5474–5495, https://doi.org/10.1039/D1AN00808K.
[6] P. Nandhikonda, M.D. Heagy, An abiotic fluorescent probe for cardiac troponin I, J. Am. Chem. Soc. 133 (2011) 14972–14974, https://doi.org/10.1021/ja205211a.
[7] Q. Liu, P. Ren, X. Wang, Y. Li, Y. Yang, Experimental and theoretical investigation of the photoelectrical properties of tetrabromophenol blue- and bromoxylenol blue-based solar cells, J. Nanomater. (2018), https://doi.org/10.1155/2018/9720595.
[8] J.L. Robinson, A.A. Venner, I. Seiden-Long, Urine protein detection by dipstick: no interference from alkalinity or specific gravity, Clin. Biochem. 71 (2019) 77–80, https://doi.org/10.1016/j.clinbiochem.2019.07.005.
[9] V. Prevot, Y. Tokudome, 3D hierarchical and porous layered double hydroxide structures: an overview of synthesis methods and applications, J. Mater. Sci. 52 (2017) 11229–11250.
[10] M.B. Poudel, H.J. Kim, Confinement of Zn-Mg-Al-layered double hydroxide and α-Fe2O3 nanorods on hollow porous carbon nanofibers: a free-standing electrode for solid-state symmetric supercapacitors, Chem. Eng. J. 429 (2022), 132345, https://doi.org/10.1016/j.cej.2021.132345.
[11] A.M. Pisoschi, A. Pop, A.I. Serban, C. Fafaneata, Electrochemical methods for ascorbic acid determination, Electrochim. Acta 121 (2014) 443–460, https://doi.org/10.1016/j.electacta.2013.12.127.
[12] W. Chen, X. Lin, L. Huang, H. Luo, Electrochemical characterization of polymerized cresol red film modified glassy carbon electrode and separation of electrocatalytic responses for ascorbic acid and dopamine oxidation, Microchim. Acta 151 (2005) 101–107.
[13] S.A. Kumar, P.H. Lo, S.M. Chen, Electrochemical selective determination of ascorbic acid at redox active polymer modified electrode derived from direct blue 71, Biosens. Bioelectron. 24 (2008) 518–523, https://doi.org/10.1016/j.bios.2008.05.007.
[14] S.B. Khoo, F. Chen, Studies of sol-gel ceramic film incorporating methylene blue on glassy carbon: an electrocatalytic system for the simultaneous determination of ascorbic and uric acids, Anal. Chem. 74 (2002) 5734–5741, https://doi.org/10.1021/ac0255882.
[15] M.A. Ahmed, A.A. Mohamed, An efficient adsorption of indigo carmine dye from aqueous solution on mesoporous Mg/Fe layered double hydroxide nanoparticles prepared by controlled sol-gel route, Chemosphere 174 (2017) 280–288, https://doi.org/10.1016/j.chemosphere.2017.01.147.
[16] C. Löwbeer, A. Gutierrez, S.A. Gustafsson, R. Norrman, J. Hulting, A. Seeberger, Elevated cardiac troponin T in peritoneal dialysis patients is associated with CRP and predicts all-cause mortality and cardiac death, Nephrol. Dial. Transplant. 17 (2002) 2178–2183, https://doi.org/10.1093/ndt/17.12.2178.
[17] I. Sarangadharan, S.L. Wang, R. Sukesan, P.C. Chen, T.Y. Dai, A.K. Pulikkathodi, C.P. Hsu, H.H.K. Chiang, L.Y.M. Liu, Y.L. Wang, Single drop whole blood diagnostics: portable biomedical sensor for cardiac troponin I detection, Anal. Chem. 90 (2018) 2867–2874, https://doi.org/10.1021/acs.analchem.7b05018.
[18] T.M. Elmorsi, M.H. Elsayed, M.F. Bakr, Enhancing the removal of methylene blue by a modified 1 ZnO nanoparticles, kinetics and equilibrium studies, Can. J. Chem. 95 (2017) 590–600, https://doi.org/10.1139/cjc-2016-0456.
[19] L. Zhang, J. Wang, J. Zhu, X. Zhang, K. San Hui, K.N. Hui, 3D porous layered double hydroxides grown on graphene as advanced electrochemical pseudocapacitor materials, J. Mater. Chem. A. 1 (2013) 9046–9053, https://doi.org/10.1039/C3TA11755C.
[20] J. Chen, Y. Sheng, Y. Song, M. Chang, X. Zhang, L. Cui, D. Meng, H. Zhu, Z. Shi, H. Zou, Multimorphology mesoporous silica nanoparticles for dye adsorption and multicolor luminescence applications, ACS Sustain. Chem. Eng. 6 (2018) 3533–3545, https://doi.org/10.1021/acssuschemeng.7b03849.
[21] G. Yang, T. Takei, S. Yanagida, N. Kumada, Enhanced supercapacitor performance based on CoAl layered double hydroxide-polyaniline hybrid electrodes manufactured using hydrothermal-electrodeposition technology, Molecules 24 (2019) 976, https://doi.org/10.3390/molecules24050976.
[22] W.B. Beshir, Radiation sensitive indicator based on tetrabromophenol blue dyed poly (vinyl alcohol) Radiat, Phys. Chem. 86 (2013) 29–135, https://doi.org/10.1016/j.radphyschem.2013.01.019.
[23] X. Wu, X. Tan, S. Yang, T. Wen, H. Guo, X. Wang, A. Xu, Coexistence of adsorption and coagulation processes of both arsenate and NOM from contaminated groundwater by nanocrystallined Mg/Al layered double hydroxides, Water Res. 47 (2013) 4159–4168, https://doi.org/10.1016/j.watres.2012.11.056.
[24] S. Chairam, W. Sriraksa, M. Amatatongchai, E. Somsook, Electrocatalytic oxidation of ascorbic acid using a poly (aniline-co-m ferrocenylaniline) modified glassy carbon electrode, Sensors 11 (2011) 10166–10179, https://doi.org/10.3390/s111110166.
[25] S.R. Ali, R.R. Parajuli, Y. Ma, Y. Balogun, H. He, Interference of ascorbic acid in the sensitive detection of dopamine by a nonoxidative sensing approach, J. Phys. Chem. B 111 (2007) 12275–12281, https://doi.org/10.1021/jp073705x.
[26] S. Tajik, M.A. Taher, H. Beitollahi, First report for simultaneous determination of methyldopa and hydrochlorothiazide using a nanostructured based electrochemical sensor, J. Electroanal. Chem. 704 (2013) 137–144, https://doi.org/10.1016/j.jelechem.2013.07.008.
[27] S. Feng, M. Yan, Y. Xue, J. Huang, X. Yang, Electrochemical immunosensor for cardiac troponin I detection based on covalent organic framework and enzyme-catalyzed signal amplification, Anal. Chem. 93 (2021) 13572–13579, https://doi.org/10.1021/acs.analchem.1c02636.
[28] H. Qi, X. Qiu, D. Xie, C. Ling, Q. Gao, C. Zhang, Ultrasensitive electrogenerated chemiluminescence peptide-based method for the determination of cardiac troponin I incorporating amplification of signal reagent-encapsulated liposomes, Anal. Chem. 85 (2013) 3886–3894, https://doi.org/10.1021/ac4005259.
[29] V. Raj, S. Alex, Non-enzymatic colorimetric sensor for cardiac Troponin I (cTnI) based on self-assembly of gold nanorods on heparin, Gold Bull. 54 (2021) 1–7, https://doi.org/10.1007/s13404-020-00287-w.
[30] M. Negahdary, H. Heli, An electrochemical troponin I peptisensor using a triangular icicle-like gold nanostructure, Biochem. Eng. J. 151 (2019), 107326, https://doi.org/10.1016/j.bej.2019.107326.
[31] H. Jo, H. Gu, W. Jeon, H. Youn, J. Her, S.K. Kim, C. Ban, Electrochemical aptasensor of cardiac troponin I for the early diagnosis of acute myocardial infarction, Anal. Chem. 87 (2015) 9869–9875, https://doi.org/10.1021/acs.analchem.5b02312.
[32] Y. Ma, X.L. Shen, H.S. Wang, J. Tao, J.Z. Huang, Q. Zeng, L.S. Wang, MIPs-graphene nanoplatelets-MWCNTs modified glassy carbon electrode for the determination of cardiac troponin I, Anal. Biochem. 520 (2017) 9–15, https://doi.org/10.1016/j.ab.2016.12.018.